Materials Science in Semiconductor Processing xxx (xxxx) 106012

Contents lists available at ScienceDirect

Materials Science in Semiconductor Processing

journal homepage: www.elsevier.com/locate/mssp

Experimental and theoretical studies on structural, morphological, electronic, optical and magnetic properties of $Zn_{1-x}Cu_xO$ thin films ($0 \leq x \leq 0.125$)

Elhadj Benrezgua [a, f], Bahri Deghfel [f, *], Abdelhafid Mahroug [b], Muhamad Kamil Yaakob [d, g], Ammar Boukhari [b, f], Rabie Amari [b, f], Soorathep Kheawhom [e], Ahmad Azmin Mohamad [c, d, **]

[a] Physics and Chemistry of Materials Lab, Department of Physics, University Mohamed Boudiaf of M'sila, 28000 M'sila, Algeria
[b] Department of Mechanical Engineering, Faculty of Technology, University of M'sila, Algeria
[c] School of Materials and Mineral Resources Engineering, Universiti Sains Malaysia, 14300, Nibong Tebal, Penang, Malaysia
[d] Ionics Materials and Devices (iMADE) Research Laboratory, Institute of Science, Universiti Teknologi MARA, 40450, Shah Alam, Malaysia
[e] Department of Chemical Engineering, Faculty of Engineering, Chulalongkorn University, Bangkok, 10330, Thailand
[f] Laboratory of Materials and Renewable Energy, Faculty of Sciences, Mohamed Boudiaf University of M'sila, 28000, M'sila, Algeria
[g] Faculty of Applied Sciences, Universiti Teknologi MARA, 40450, Shah Alam, Malaysia

ARTICLE INFO

Keywords:
Copper-doped zinc oxide thin films
Density functional theory
Ferromagnetic phase
Sol-gel technique
Spin coating method
LDA + U approach

ABSTRACT

Pure and copper-doped zinc oxide thin films at different contents *x* ($Zn_{1-x}Cu_xO$; $0 \leq x \leq 0.125$) were synthesized by sol–gel spin coating process and investigated using various techniques. All samples exhibited a polycrystalline with wurtzite hexagonal phase, which wasn't altered and getting relaxed by Cu-doping. The grain size increased and changed its growth mode from c-axis growth to lateral one and the surface morphology was strongly influenced with increasing level of Cu doping. As *x* increased, the transparency of films was generally increased in the visible region and the band gap energy (*Eg*) presented a slight shrinking, indicating that the prepared films are suitable for use in opto-electronic applications. Ferromagnetic phase was adopted within density functional theory corrected by Hubbard method (DFT + LDA + U) to investigate the structural, electronic, magnetic and optical properties of pure and CZO structure. The closest Cu impurities gave the more stable configuration. Cu3d states were distributed around Fermi level inducing a major contribution to the magnetic moment. A mix of ionic and covalent bonding was remarked. DFT + LDA + U enhanced significantly the calculated *Eg*, which presented a narrowing with *x*. The imaginary part of the dielectric functions presented three main peaks and their static constants were slightly influenced by Cu doping.

1. Introduction

In the last decade there has been an increasing interest in Zinc oxide (ZnO) doped with transition metal (TM; i.e., Mn, Fe, Co, Ni, Cu and Ag) [1]. This is due to its recognized potential in many applications. Among the variety of TM, copper (Cu) has been used as dopant [2–4]. It exhibits an ionic radii close to that of the Zn and then can easily substitute it in ZnO host lattice. Cu dopant, as an economical option, has been chosen to enhance the properties of ZnO host lattice such as photocatalytic activity, conductivity and tuning of the green emission [5,6].

ZnO thin films have been fabricated by many techniques like magnetron sputtering [7], sol–gel process [8,9], chemical vapor deposition [10], spray pyrolysis [11], molecular beam epitaxy [12], pulsed laser deposition (PLD) [13] and microwave plasma growth [14]. Sol–gel technique attracts much attention because of its advantages including safety, low cost, simple deposition equipment on a large-area films with uniform thickness. Properties of copper-doped zinc oxide thin films (CZO) at different contents *x* ($0 \leq x \leq 0.125$) thin films have been frequently investigated [15–26]. However, most of the published articles are restricted to low Cu-doping and some elaboration methods.

To achieve a prior knowledge on the properties of materials, a theoretical framework are needed. Plane-wave pseudopotential (PWPP) density functional theory (DFT) has been successfully used to predict the electronic ground states. Moreover, the localization of strongly cor-

* Corresponding author: bahri.deghfel@univ-msila.dz (DB)
** Corresponding author: aam@usm.my (AAM)
E-mail addresses: bahri.deghfel@univ-msila.dz (B. Deghfel), aam@usm.my (A.A. Mohamad).

https://doi.org/10.1016/j.mssp.2021.106012
Received 3 January 2021; Received in revised form 23 May 2021; Accepted 7 June 2021
1369-8001/

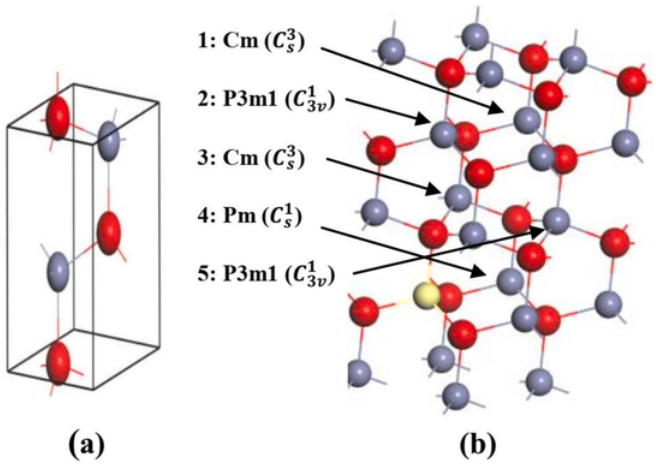

Fig. 1. ZnO primive cell (a) and 2 × 2 × 2 ZnO supercell (b): O atoms are in red, the first Cu atom (yellow) is taken to be fixed and the second one substitutes Zn atom (gray) at different geometry configurations for x = 12.5%. (For interpretation of the references to color in this figure legend, the reader is referred to the Web version of this article.)

related *d* and *f* electrons of the metal oxides are not well described by the traditional theory DFT, which underestimates their band gap [27]. Thus, DFT–LDA + U approach becomes a necessity to significantly improve such calculations [27–30]. There have been several theoretical studies on Cu-doped ZnO [31–43], which have provided some new insights into the understanding of the effect of doping on the properties of ZnO. However, the calculated band gap of CZO was found much smaller than the experimental band gap value, although some studies have used the DFT + U approach. So, further calculations with convenient Hubbard U values are still justified to enhance the band gap, which is the main motivation for the present work.

There have been several experimental studies on Cu-doped ZnO. However, most of these studies are restricted to low Cu-doping of ZnO thin films. The present study is devoted to the fabrication of pure ZnO and copper-doped zinc oxide (CZO) thin films with somewhat higher Cu contents (x) (x = 1%, 3.12%, 6,25% and 12.5%) and low thickness. The structural, morphological, electronic and optical properties of CZO thin films are then characterized using various techniques. In order to linking of experimental results with theory, usually separated in the literature, and to enhance the energy band gap, DFT–LDA + U approach was used to predict the properties of pure and CZO wurtzite structures, which were compared, wherever possible, with their corresponding measured values.

2. Computational and experimental details

First-principles calculations of structural, electronic, magnetic and optical properties of pure and CZO wurtzite materials (x = 6,25%, 12.5%) were performed by DFT as implemented in CASTEP code [44]. The generalized gradient approximation (GGA) in the scheme of Perdew–Burke–Ernzerhof (PBE) was employed to describe the exchange-correlation function [45]. 2 × 2 × 4 and 2 × 2 × 2 ZnO supercell model, derived from the optimized ZnO primitive cell (Fig. 1 (a)), and substitutional method [46] were used to achieve the considered Cu content of 6,25% and 12.5%, respectively (Fig. 1(b)). The valence-electron configurations for the O, Zn and Cu atoms are chosen as $2s^2\ 2p^4$, $3\ d^{10}\ 4s^2$ and $3\ d^{10}\ 4s^1$, respectively. The energy cut-off was fixed at 400 eV, which is enough to perform the present calculation with plane-wave ultrasoft pseudopotential method [47]. The Brillouin zone is sampled by k-point meshes of 3 × 3 × 1 and 5 × 5 × 3 for 2 × 2 × 4 and 2 × 2 × 2 ZnO supercell, respectively. The optimization convergence for maximum force, energy change, maximum displacement and maximum stress were fixed at 0.05 eV/Å, 5 × 10^{-6} eV/atom, 10 × 10^{-4} Å and 0.05 GPa, respectively. The SCF convergence threshold was 5.0 10^{-6} eV per atom.

The semiempirical LDA + U approach [27] was used with effective Hubbard U values of 5.5, 6.0 and 8.0 eV for Zn *3d, Cu 3d and O 2p* electrons, respectively. Furthermore, ferromagnetic phase of CZO (x = 6.25% and 12.5%) was adopted in which two Cu atoms substitute two Zn atoms according to five different geometry configurations (Fig. 1); for x = 12.5%, the first Cu atom is taken to be fixed and the other Cu atom changes its place. The ferromagnetic phase adopted here was supported by previous studies [36,48].

Experimentally, Copper (II) chloride [$CuCl_2{\cdot}2H_2O$], Zinc acetate dihydrate [Zn $(CH_3COO)_2.2H_2O$] and 2-Methoxyethanol were used as a dopant source and starting material and stabilizer, respectively, to prepare pure and CZO thin films (x = 1%, 3.12%, 6.25%, 12.5%) on glass substrates using sol–gel spin coating method. The concentration of metal ions was fixed at 0.6 M and the molar ratio of the solvent (Monoethanolamine-MEA) to metal ions was 1.0. After stirring at 65 °C for 2 h, the solution was then aged at room temperature for 24 h. The solution was deposited on a clean and dry substrate at a rate of 2800 rpm for 30 s. The films were then preheated at 250 °C for 10 min. These tow last processes were repeated several times. The obtained films were finally annealed for 1.5 h at 480 °C. In order to have the desired content of Cu dopant in the range from 0 to 12.5 at.%, the precursors are mixed together with different appropriate molar ratios as described in Ref. [49] for low concentrations. Also, the Copper (II) chloride [$CuCl_2{\cdot}2H_2O$] was used instead of copper (II) nitrate trihydrate (Cu (NO3)2·3H2O) as source of Cu.

Many techniques were employed to investigate the fabricated samples such as X-ray diffractometer XRD (Broker advanceSolution D8 X-ray diffractometer with Cu-kα radiation λ = 1.5406 A°), Atomic Force Microscopy AFM (NanoNavi/SPA 400), Field emission scanning electron microscopy FESEM (Carl Zeiss Aurga) and Ultraviolet–visible UV–vis spectrophotometer (VARIAN Carry 50).

3. Results and discussion

3.1. Experimental results

The XRD pattern (Fig. 2(a)) confirms the formation of polycrystalline with wurtzite hexagonal phase for pure and CZO thin films (x = 1, 3.12, 6,25 and 12.5%). No other phases are observed, indicating that hexagonal wurtzite structure of ZnO films isn't altered by Cu-doping. Unlike the intensity of (002) peak, the intensity of (100) and (101) peaks are generally enhanced, especially at high Cu-doping, which leads to the degradation of the (002) preferential orientation of ZnO thin films. Similar results have also been reported earlier for CZO in other reports using various techniques; Syed Zahirullah et al. (thin films with x up to 10%) [15], Saidani et al. (thin films with 1 wt% ≤x ≤ 5 wt%) [16], Osali et al. (thin films with 0 wt% ≤x ≤ 6 wt%) [17], Sreedhar et al. (thin films with 0 at.% ≤x ≤ 7.5 at.%) [18], Joshi et al. (thin films with 0 at.% ≤x ≤ 10 at.%) [19]. However, some other workers found that a CuO phase has been appeared with emerging a (111) new peak at high Cu doping; x = 10 at.% [19], x ≥ 15 at.% [20] or even at low Cu doping [21].

The lattice constants $a = b$ and c for pure and CZO thin films are calculated using XRD patterns (Table 1). It is found that both $a = b$ and c are slightly decreased with Cu content. This is due to incorporation of Cu into ZnO host lattice where the ionic radius of Cu^{2+}(0.73A°) is slightly smaller than that of Zn^{2+} (0.74A°).

The lattice strain ε is estimated using the formula $\varepsilon = \beta\cos\theta/4$, where β is the full width at half maximum of the corresponding peak [17]. In addition, The Scherrer formula $D = K\lambda/\beta\cos\theta$ was used to estimate the average crystallite size (D), where K is the shape factor (K = 0.9), λ is the X-ray wavelength (λ = 1.5406 Å), β is the full width at half maxima of a given diffraction peak and θ is the Bragg angle [17].

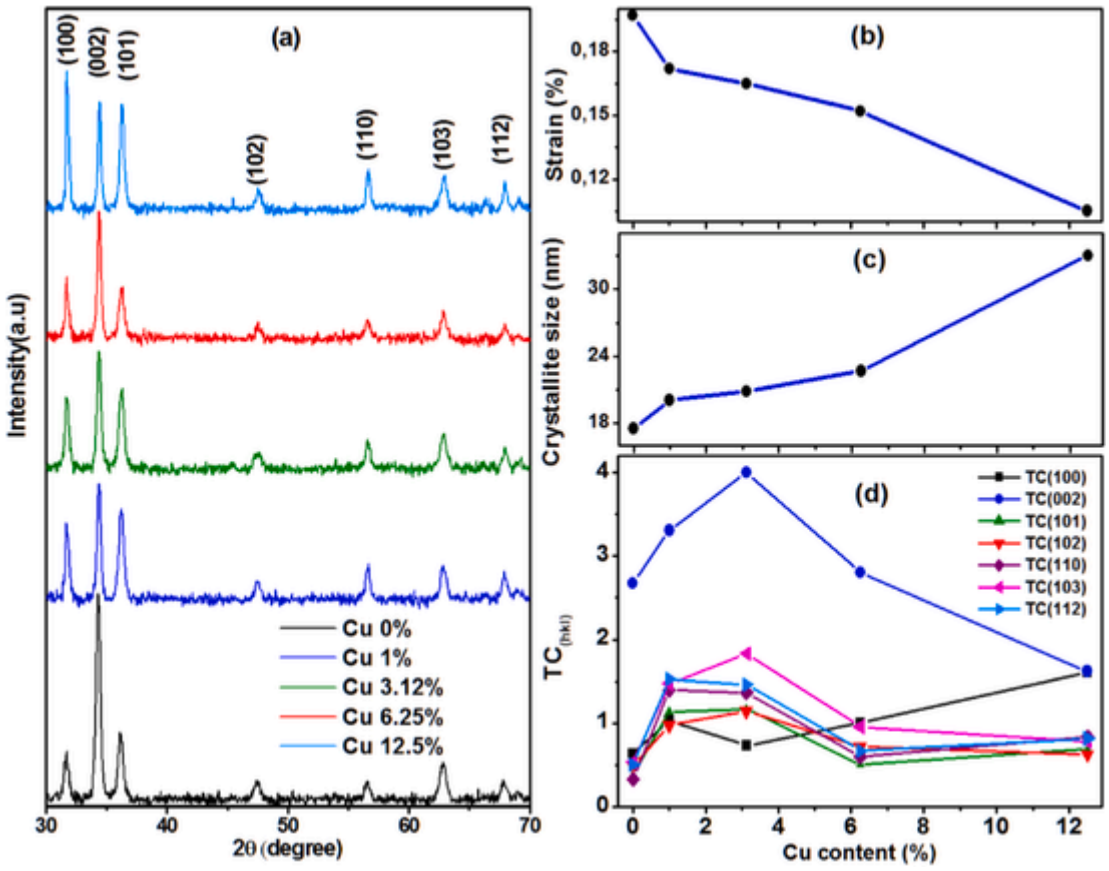

Fig. 2. X-ray diffraction patterns (a), Strain (b), crystallite size (c) and texture coefficient (d) of pure and CZO thin films (x = 1, 3.12, 6,25 and 12.5%).

Table 1
Structural and optical parameters of pure and CZO thin films (x = 1, 3.12, 6.25, 12.5%).

x (%)	2θ (°)	c (Å)	a (Å)	FWHM (°)	Peak intensity	Grain size (AFM) (nm)	Thickness (nm)	*Rrms* (nm)	ε_o (n_o)
0	34.43	5.205	3.249	0.4731	(002)	74.22	357	116.78	4.517 (2.125)
1	34.37	5.213	3.257	0.4141	(002)	78.76	350	129.45	3.443 (1855)
3.12	34.38	5.212	3.257	0.3982	(002)	85.94	343	157.76	3.378 (1.838)
6.25	34.40	5.209	3.254	0.3664	(002)	105.47	332	186.00	3.376 (1.837)
12.5	31.75	5.203	3.251	0.2498	(100)	117.19	318	209.52	2.736 (1.654)

Undoped thin films possess a high strain value which goes on decreasing as x increases (Fig. 2(b)), suggesting that the films are getting relaxed due to replacement of the host (Zn^{2+}) by the dopant (Cu^{2+}) cations. Lee et al. [25] observed the same behavior, who explained this phenomenon by the presence of excess Cu dopant located at grain boundaries.

The obtained crystallite size increases with increasing Cu doping (Fig. 2(c)). Similar behavior was also tabulated in the literature: Joshi et al. [19] observed an increase from 33.06 nm to 43.65 nm for Cu doping from 0% to 10%, Shewale et al. [23] estimated a crystallite size values of around 37.47 nm and 48.28 nm for undoped and 2 at.% CZO thin films, while Chen et al. [24] noticed an increase from 20 to 50 nm and then a decrease to 29 nm for Cu content of 2%, 6%, and 10%, respectively.

To investigate the texture of a given plane, the texture coefficient ($TC_{(hkl)}$) is needed. This coefficient is estimated by using $TC_{(hkl)} = I_{(hkl)}/I_{0(hkl)}/\left(\sum_1^N I_{(hkl)}/I_{0(hkl)}/N\right)$, where $I\,(hkl)$ and $I_0\,(hkl)$ are the measured relative intensity of a diffraction peak and the intensity of the standard powder diffraction peak taken from the JCPDS data, respectively, and N is the number of diffraction peaks [8]. The higher values of TC (greater than unity) for a given (hkl) direction indicate the abundance of crystallites in this direction. The TC values are presented as function of Cu doping for all peaks observed in the XRD pattern (Fig. 2(d)). It is observed that all films present highest TC values for (002) plane indicating a preferred growth along c-axis, which is converted to (100) plane for higher Cu content. This does mean that the degree of preferred growth orientation of the prepared thin films depends on the Cu concentration. Also, the higher value of texture coefficient reveals a better crystallinity of the prepared thin films. These findings are in agreement with the obtained crystallite size.

The energy dispersive spectroscopy (EDS) technique is used to confirm the presence of Cu in ZnO thin film. EDX spectra of pure ZnO (Fig. 3(a)) and CZO thin films with x = 6.25% (Figs. 3(b)) and 12.5% (Fig. 3(c)) are shown. The EDX spectrum of all samples exhibits an oxygen peak at around 0.529 keV and a Zinc peak at around 1.009 KeV. However, extra peak at around 0.939 KeV corresponding to the copper is also revealed together with the previous observed peaks for CZO thin films. Other peaks are also observed indicating the presence of other elements such as Si and C, which belong to the glass substrate and other residues. The significant decrease in Zn peak intensity with Cu doping is accompanied with the increase of its coinciding Cu peak intensity. Besides, the O peak intensity is still unchanged with Cu doping. This clearly suggests that Zn has been successfully substituted by Cu into the ZnO host lattice. Based on these findings, it is possible to suppose the

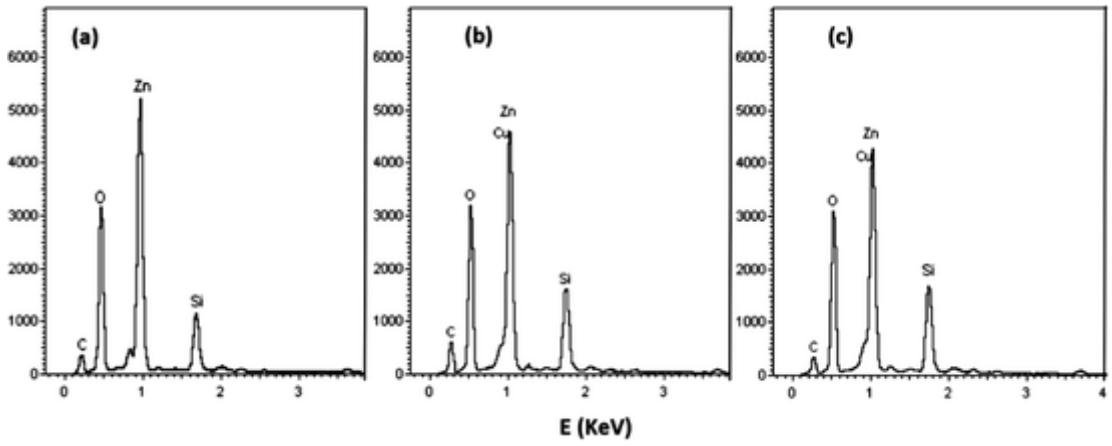

Fig. 3. EDX spectra of pure ZnO (a) and CZO thin films; x = 6.25% (b), 12.5% (c).

stoichiometric films of the form $Zn_{1-x}Cu_xO$ [20]. Then, it is found from the quantitative analysis that the Cu concentrations of 8.56% and 10.81% are comparable to the actual Cu doping contents of 6.25% and 12.5% added during the preparation.

1.0 × 1.0 μm^2 two and three-dimensional AFM images are shown for pure and CZO thin films with Cu content of 1, 3.12, 6,25 and 12.5% (Fig. 4 a, b, c, d and e). The grains, extracted using WsXM software [50], are round shape (two dimensional AFM images) and their average size increases with Cu doping (Table 1). This is consistent with the changes occurred in (002) preferential orientation observed from XRD patterns, where the growth mode of grains translates from c-axis growth perpendicular to the substrate to the lateral one with increasing level of Cu doping. The pure ZnO films exhibit smooth surface. However, surface morphology is strongly influenced by the Cu doping and the surface becomes rough (three-dimensional AFM images), which is traduced by the increasing values of the root mean squared roughness (Table 1). The results of root mean squared roughness and average grain size are found to be consistent, i.e. thin films with small grain size exhibit a smooth surface. Joshi et al. [19] remarked an increase in both crystallite size and grain size and a decrease in strain with Cu doping. Sreedhar et al. [18] also reported results which exhibit a similar behavior except at high Cu concentration. Hashim et al. [21] reported that the type of substrate also affected the grain growth and shape. Salem et al. [51] noticed that the high doping concentration can lead to large grain size and rough surface morphology.

Field emission scanning electron microscopy (FESEM) 2D images and their corresponding cross-section images of pure ZnO and CZO thin films are shown (Fig. 4(f, g, h, i) and j). All the FESEM images were obtained at 20,000 × magnifications. It can be seen from these images that the morphology shows irregular sized aggregated clusters for pure ZnO, while it exhibits a randomly distributed mixer of spheroid-like and rod-like nanoparticles (granules) for CZO thin films. Moreover, the particles tend to agglomerate together to form large clusters (agglomerates) by increasing x. These agglomerates are held together by weaker forces arising from electrostatics, Van der Waals, solvation or capillary effects [52], in such case the Cu doping play an important role to strengthen these forces. The film thicknesses, estimated from cross-section images, were found to be about 318–357 nm, which seem slightly changed by Cu doping (Table 1). These findings are in agreement with other previous results [20,53–55]. Some other reports noticed no change in the film thickness with increasing level of Cu concentration [24,56].

The absorbance (A) ($A = 1 - R - T$) of CZO thin films is calculated from measured transmittance (T) and reflectance (R) spectra [57]. The absorption coefficient α ($\alpha = 2.303\ A/d$)is then calculated for the sample with thickness d. For measurement with normal incidence, the extinction coefficient k ($k = \alpha\lambda/4\pi$) and the refractive index n ($n = (1+R)/(1-R) + \sqrt{4R/(1-R)^2 - k^2}$) of film can then be determined for the incident wavelength (λ) from the surface of the sample. The real ε_1 ($\varepsilon_1 = n^2 - k^2$) and imaginary ε_2 ($\varepsilon_2 = 2nk$) parts of the complex dielectric function can also be estimated.

The transmission spectra of pure and CZO thin films in the wavelength range 350–1000 nm (Fig. 5(a)), were also exploited to deduce the band gap Eg Refs. [58,59]. It can be seen that the transparency of films generally increases from 72% to 80% in the visible region with increasing of x. This is due to the increase of grain size with Cu doping, which leads to reducing the grain boundary density or scattering centers. Saidani et al. [16] found that the transmittance have increased from 77% to 92% when the concentration of Cu was increased from 0% to 5 wt%. Sreedhar et al. [18] also measured a transmission greater than 83% for Cu doping less than 6.2 at.% and transmission of 80% for Cu doping of 7.5 at.%. The observed sharp absorption edge in the UV region (350–400 nm) for all films shifts to longer wavelengths by increasing Cu content leading to the decrease in the experimental band gap energy from 3.34 eV to 3.25 eV. Similar trend has been observed for ZnO thin films prepared at various Cu-doping range [15,17,18,20,22,24,26,51,60–62].

The dependence of the optical parameters (α, k, n, ε_1 and ε_2) on the photon energy is presented for pure and CZO thin films (Fig. 5(b), (c) and (d)). The dispersion formulae of DiDomenico and Wemple [63] is commonly used to calculate the refractive index in $E = h\nu < Eg$ range, where E is the photon energy. In such formulae the factors $1/(n^2\text{-}1)$ are plotted versus photon energy squared (E^2). Using straight line fitting technique to these plots (Inset in Fig. 5(c)), static refractive index $n_0 = (1 + E_d/E_o)^{1/2}$ (n when $E \sim 0$, where E_d *and* E_o are the dispersion energy and the average oscillator energy, respectively) and static dielectric constant $\varepsilon_o = (n_o)^2$ are then estimated for CZO thin films (Table 1). E_o/Ed is the intercept of the straight line fitting and $-1/(E_oEd)$ is its slope.

The analysis shows that the value of absorption coefficient is still invariant with the increase in the incident energy for all thin films up to a certain value in the visible region (optical absorption edges) depending on the Cu doping. After that, α increases sharply and generally shifts to lower values of energy with Cu doping, which predicts a decrease in the band gap energy. The refractive index is found to be increased with energy in the visible light range and sensitive to Cu dopant concentration. Also, static refractive index n_0 decreases with Cu doping. This may be due to the decrease in film density caused by the increase in crystallite size (Table 1). These findings are in agreement with those reported by other researchers for pure ZnO [57,64,65] and CZO thin films [55]. Furthermore, the dielectric function follow the same pattern as the refractive index from which is derived.

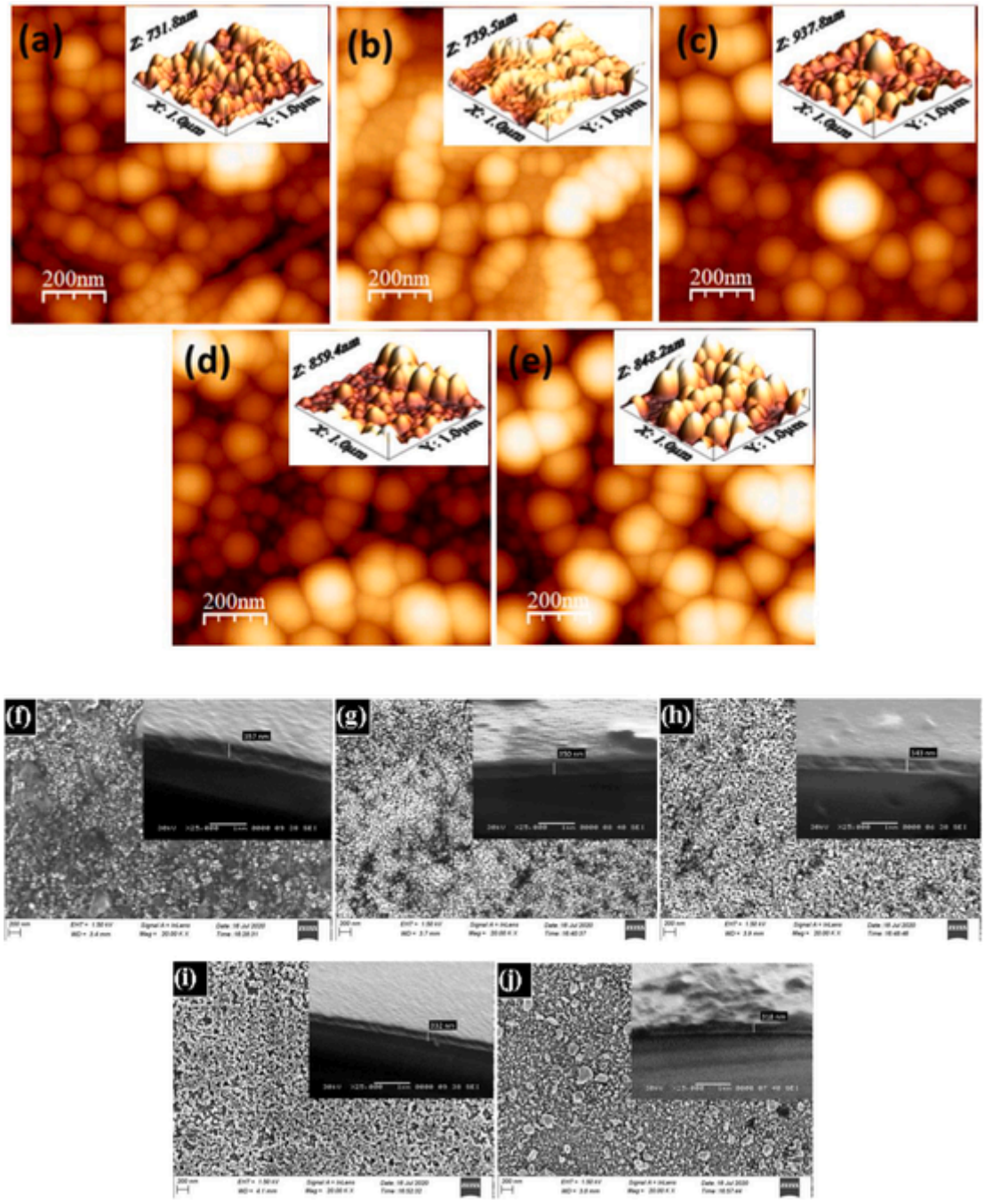

Fig. 4. 1.0 × 1.0 μm^2 Two and three-dimensional AFM images of thin films for x = 0% (a), 1% (b), 3.12% (c), 6.25% (d) and 12.5% (e) and FESEM 2D images and their corresponding cross-section images of thin films for x = 0% (f), 1% (g), 3.12% (h), 6.25% (i) and 12.5% (j).

3.2. DFT + U calculations

The difference in total energy ($\Delta E_i = E_i - E_3$; $i = 1,..5$) corresponding to third geometry configuration (E_3), taken as an energy reference, is estimated for the various geometry configurations from substitution of Zn by Cu, marked as 1, 2, 3, 4 and 5. The values of ΔE_i are summarized for CZO (x = 12.5%) as follows; $\Delta E_1 = 0.5\ meV$, $\Delta E_2 = 4.1\ meV$, $\Delta E_3 = 0.0\ meV$, $\Delta E_4 = 17.6\ meV$ and $\Delta E_1 = 2.0\ meV$ corresponding to the distance between two Cu atoms ($d_i = d_{Cu_{Fix}-Cu_i}$; $i = 1,..5$, Cu_{Fix} denotes fixed Cu atom) $d_1 = 6.112$ A°, $d_2 = 5.181$ A° , $d_3 = 3.199$ A°, $d_4 = 3.243$ A° and $d_5 = 4.552$ A°, respectively. This does mean that the third configuration (symmetry group Cm (C_s^3)) is the more stable state (ground state) where Cu atoms are at a short distance around the O atom. This agrees with the results reported by Estrada et al. [48], Nayek et al. [34] and Wang et al. [40]. The configuration corresponding to the stable state will also be considered for studying the effect of the Hubbard U values on the band gap energy.

Based on previous studies [28,31–33], we focus on the effective Hubbard U values for *Cu 3d* state, which was found to be distributed around Fermi level and it was responsible for the shrinking of the band gap. The increase of effective Hubbard U values for *Cu 3d* state tends to enhance significantly the calculated electronic energy gap (*Eg*) compared to that deduced from experiment; U *Cu 3d* = 6, 8 and 10 eV give *Eg* = 1.860, 2.537 and 3.315 eV, respectively, for Cu-doped ZnO (x = 12.5%). Furthermore, U *Cu 3d* = 10 eV gives *Eg* = 3.380 and 3.328 eV for pure and Cu-doped ZnO (x = 6.25%). This enhancement in *Eg* is due to the improved localization of *Cu 3d* states. Then, the effective Hubbard U values of 5.5, 10 and 8eV for Zn *3d, Cu 3d and O 2p* elec-

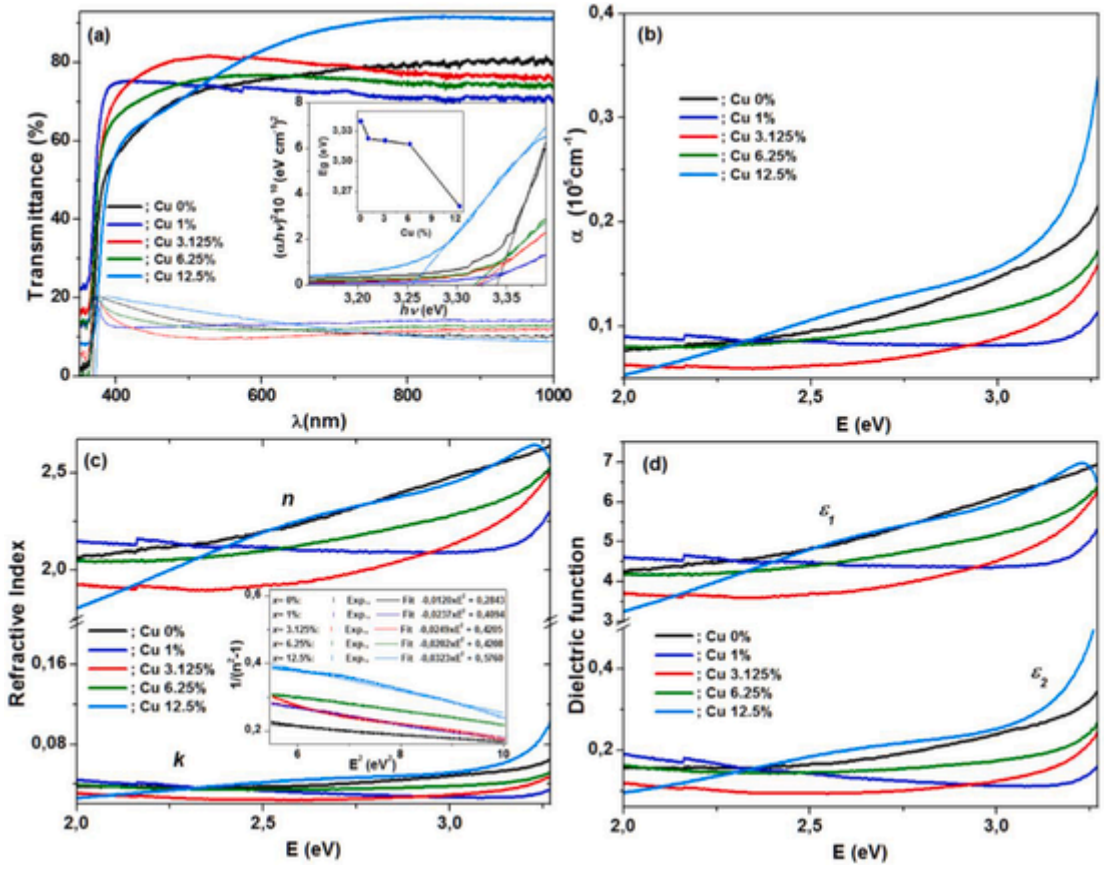

Fig. 5. Optical transmission and reflectance spectra (a), absorption coefficient (b), complex refractive index (c) and dielectric function (d) of pure and CZO thin films (x = 1%, 3.12%, 6,25%, 12.5%). Inset in (a) shows $(\alpha h\nu)^2$ versus photon energy $h\nu$ and band gap versus Cu content. Inset in (c) shows $1/(n^2\text{-}1)$ versus photon energy squared (E^2) and its fitting for different Cu content of CZO thin films.

trons, respectively, will be taken into account to evaluate the theoretical properties of the CZO structure. Earlier calculations of band gap have been reported in the literature [31,32,34–39,41], but most of them exhibited underestimation of the experimental band gaps of semi conductors. So, further calculations with convenient Hubbard U values are still justified to enhance the band gap. The present findings of band gap from theoretical calculation are in good agreement with the present experimental values (maximum relative deviation does not exceed 1.96%), in which a direct band gap is observed for pure and CZO structure (Fig. 6 middle). It confirms that the Cu doping can induce narrowing in the band gap where the bottom of the conduction band is mainly originated from Cu spin down states while Cu spin up states shift deeply into the bottom of the valence band (Fig. 6 right). This has also been observed by Fang et al. [36].

The partial density of Zn 4s, Zn 3d, Cu 4s, Cu 3d, O 2s and O 2p spin up and down states (PDOS) for pure and CZO wurtzite structures (x = 6,25%, 12.5%) are shown (Fig. 6 left). The valence band states is mainly originated from a strong mixing among the Zn3d and O2p states. The valence band states are extended down to −7.8 eV and −9.2 eV for pure and CZO structure, respectively, while Cu3d states contribution is appeared in the bottom of valence band for the doped case. This large region is followed by a narrow band, centered at −14.6 eV and unaffected by Cu doping, which is mainly originated from O2s orbitals with a weak mixing between the Zn3d and Zn4s states. The downward shift of the conduction band, dominated by Zn4s with a little contribution of Cu3d states near the Fermi level (Inset in Fig. 6), leads to the decrease of the optical band gap with the increase of x. It is also found that Cu3d states were found to be distributed around Fermi level for Cu-doped structures (x = 6,25%, 12.5%) with ferromagnetic phase in which Cu atoms are close to each other around the O atom.

Spin-polarized calculations indicate that the Cu doping induces a magnetic moment of about 0.96 μ_B/Cu with a small contribution from its nearest-neighboring O atom (0.04 μ_B/O) (Fig. 7 (a)). Magnetic moment value from our calculation is in agreement with that deduced from exchange split and crystal field theories. The splitting of the Cu^{+2} d-states in the wurtzite structure (Cu atom is tetrahedrally surrounded by four oxygen atoms) is due to exchange split into spin up and spin down states and crystal field split into a doublet and a triplet (Fig. 7 (b)). This configuration leads to a net spin equal 1 μ_B/Cu [66].

The charge density difference of slice containing Cu atoms and their neighbors ((010) surface) for pure and CZO structures, is mapped (Fig. 7 (c)). Blue, yellow and red colors indicate a region with charge accumulation (around O atom), minimal difference and charge loss (around Zn or Cu atom), respectively. The charge density difference demonstrates that the atom with high electronegativity tends to attract more electrons and vice versa (Zn:1.7, Cu:1.8 and O:3.5). This is consistent with the values of the average Mulliken atomic and bond populations (Table 2). The difference between the formal ionic charge and the calculated effective valence charge refers to the mix of ionic and covalent bonding in both pure and CZO structures (x = 6,25%, 12.5%) with more covalency for Cu–O bonds than Zn–O ones, which is consistent with the charge density difference, i.e. the smaller the charge density difference, the smaller the charge loss. This covalency decreases with Cu doping. .

Unlike the optimized lattice constant a = b, the lattice constant c is slightly decreased with Cu concentration (Table 2). Both optimized lattice constants exhibit an excellent comparison to the experimental ones; the maximum relative deviation is 0.46% and 0.21% for a = b and c,

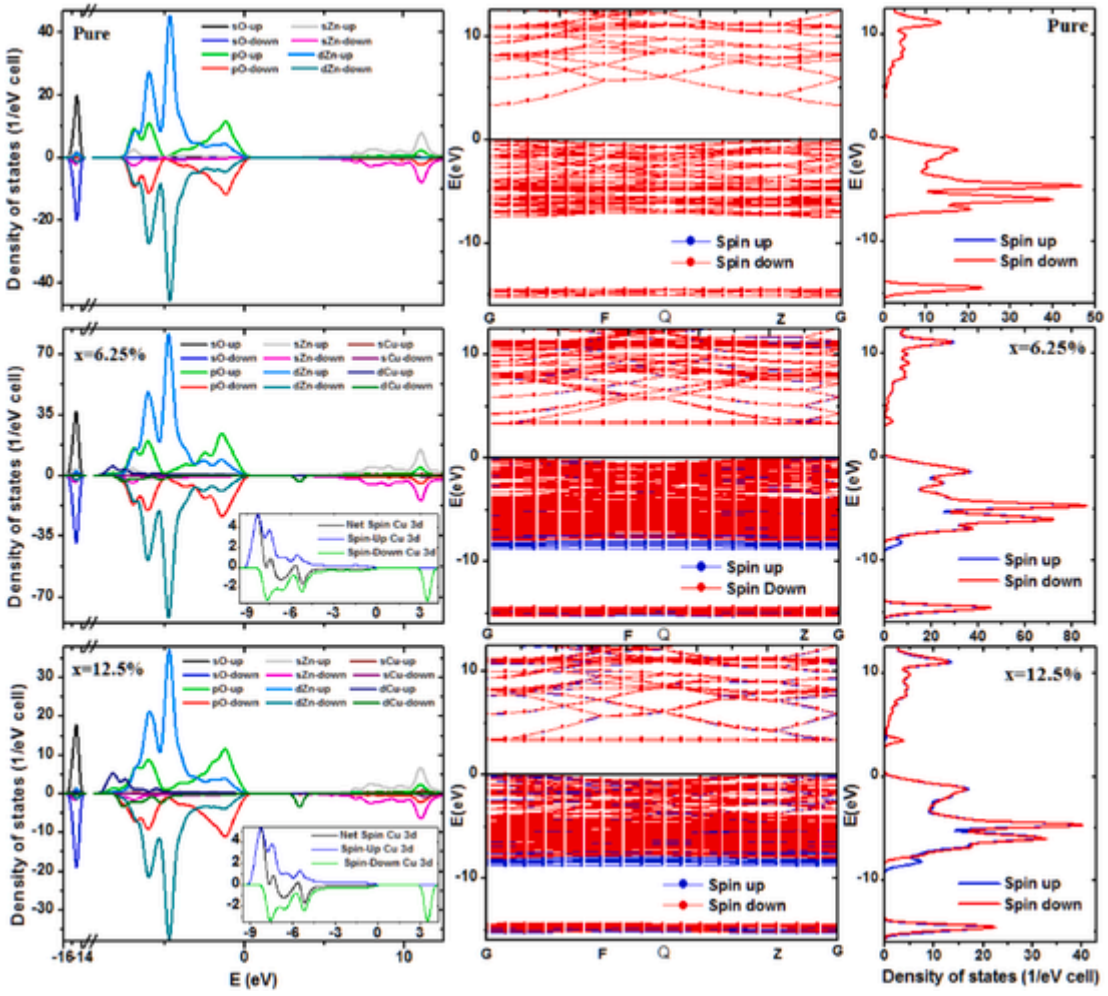

Fig. 6. PDOS of Zn 4s, Zn 3d, Cu 4s, Cu 3d, O 2s and O 2p spin up and down states (left panels), band structures (middle panels) and their corresponding spin up (blue) and spin down (red) total density of states (right panels) of pure and CZO wurtzite structures (x = 6,25%, 12.5%). Insets in PDOS show Cu 3d spin up, spin down and net spin states near Fermi level for CZO wurtzite structures (x = 6,25% and 12.5%). (For interpretation of the references to color in this figure legend, the reader is referred to the Web version of this article.)

respectively. The decrease in lattice constant c is consistent with our results extracted from XRD patterns. This decrease has been also observed by Zhao et al. [41]. In addition, the bond length was slightly changed when going from pure ZnO to Cu-doped structure, because of the comparable sizes of Zn and Cu atoms. Similar change has been found by Nayek et al. [34].

The calculated complex dielectric function is presented (Fig. 8(a)) for pure and CZO structures (x = 6,25 and 12.5%). The imaginary part consists of three main peaks. Generally, the first peak, located at around ~ 5 eV eV, corresponds to electron excitation of O-*2p* state to Zn-*4s* state or Cu-*3d* state. The intensity of this peak is slightly increased with Cu doping because of the replacement of Zn atoms by Cu ones. The second peak, located at around ~9.9 eV eV, results from electron excitation of Zn-*3d* state near the top of valence band to O-*2p* state near the bottom of conduction band. Similar results were observed by Xia et al. [35] and Lon et al. [41] and further explanations can be found therein. The excitation of Zn-*3d* state to O-*2s* state constitutes the third strong peak, which is located at around ~14.9 eV eV and decreases with Cu doping. This causes the decrease of Zn-*3d* states which are responsible for the concerned transition. Besides, an inappreciable shift of dielectric function toward the lower energy is due to the slight shrinking of band gap energy when going from pure structure to doped one. Also, the calculated static dielectric function ε_1 (0) is slightly affected by Cu doping; ε_1 (0) = 2.455 for x = 0%, 2.457 for x = 6.25% and 2.454 for x = 12.5% (Inset in Fig. 8(a)) while a significant change is observed for the experimental static dielectric function (Table 1). This may be due to the surface morphology not taken into account in the DFT + LDA + U calculations. Other optical properties, such as complex refractive index (Fig. 8(b)), complex conductivity function (Fig. 8(c)) absorption coefficient (Fig. 8(d)), optical reflectivity (Fig. 8(e)) and energy-loss function (Fig. 8(f)) are also presented. It is observed that the absorption is near zero below absorption edges, which correspond to the band gap values, and presents tow more pronounced peaks at about 16.6 and 34.6 eV. Furthermore, the strong peak of the energy loss function (around 22.0 eV) corresponds to the abrupt reduction of the reflectivity. The refractive index seems unchanged by Cu doping (around 1.56) and tends to be constant for lower photon energy in the visible light range (Inset in Fig. 8(b)), which is inconsistent with the experimental findings (Table 1). In addition, the refractive index and the absorption coefficient exhibit a similar behavior to those obtained experimentally in this work within the considered energy range (energy corresponding to the visible range).

4. Conclusion

Experimental and theoretical investigations of pure and CZO thin films are performed. Structural results show that all samples exhibited a polycrystalline with wurtzite hexagonal phase. The (002) preferential orientation is degraded and leads to the enhancement along (100) orientation by increasing Cu-doping. The crystallite size, strain and

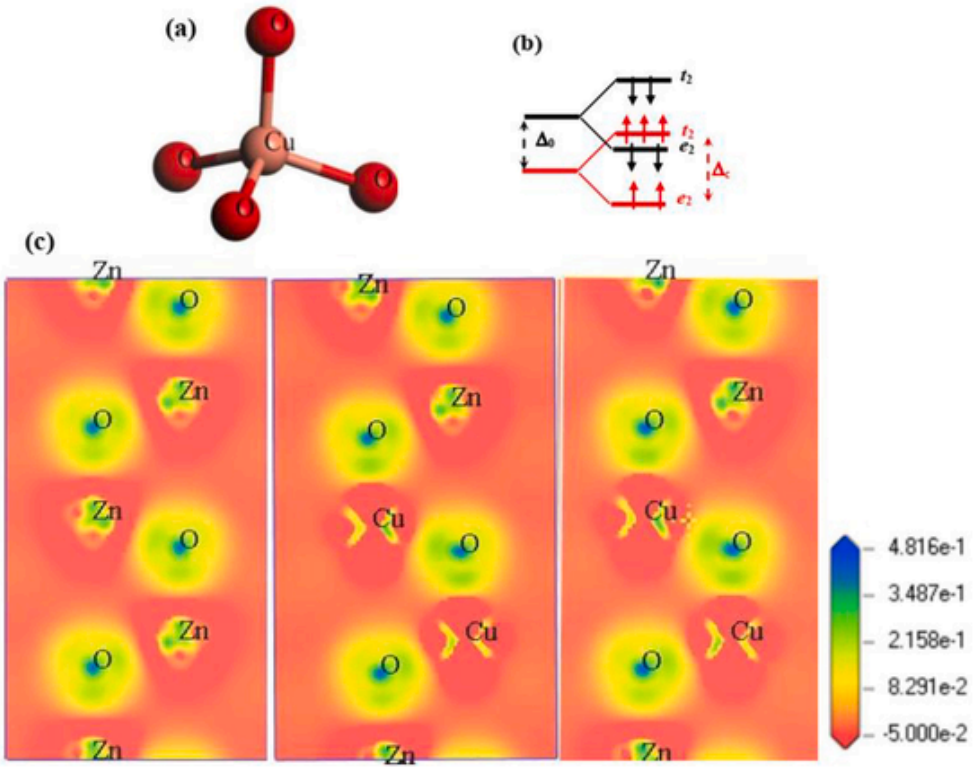

Fig. 7. Oxygen atoms are arranged with tetrahedral symmetry around copper atom in the wurtzite structure (a), exchange splitting (Δ_0) and crystal field splitting (Δ_c) into a doublet (e_2) and a triplet (t_2) Cu^{+2} d-states (b), distribution (010) surface of charge density difference for pure and CZO structures (c).

Table 2
Average Mulliken atomic, effective valence, bond populations, bond length and lattice constants of pure and CZO wurtzite structures (x = 6,25 and 12.5%).

x (%)	Atomic Population (e)			Effective valence (e)		Bond Population (e)		Bond length (A°)		Lattice constants (A°)	
	Zn	Cu	O	Zn	Cu	Zn–O	Cu–O	Zn–O	Cu–O	$a = b$	c
0	0.950	–	−0.950	1.050	–	0.402	–	1.9717	–	3.236	5.204
6.25	0,967	0.690	−0.949	1.033	1.310	0.397	0.430	1.9721	1.9785	3.239	5.199
12.5	0.985	0.705	−0.949	1.015	1.295	0.395	0.425	1.9724	1.9791	3.243	5.192

growth mode are significantly influenced by the increasing level of Cu doping. Surface morphology reveals that grain size is strongly affected by the Cu-doping and the surface becomes more rough. The film thickness is slightly influenced by Cu doping. The transparency of films presents an increase in the visible region and the band gap energy slightly shrinks as the Cu content increases, indicating that the doping process by Cu makes these films suitable for use in opto-electronic devices, in which CZO thin films can absorb the ultra violet wave range in the spectrum and it is transparent to visible light.

Calculations reveal that DFT + U with convenient effective Hubbard U values enhance the band gap. The ferromagnetic ground states at a geometry configuration with the closest Cu impurities in CZO structure is found the more stable and Cu3d states are distributed around Fermi level. Besides, the covalency for both Cu–O and Zn–O bonds is affected by Cu doping. The imaginary part consists of three main peaks whose intensity is slightly influenced by impurity doping. The static refractive index is found unchanged by Cu doping.

Author statement

Benrezgua Elhadj: Data curation, Writing – original draft. Deghfel Bahri: Methodology, Software; Abdelhafid Mahroug: Methodology, Software; Ammar Boukhari: Visualization, Investigation, Software; Rabie Amari: Visualization, Investigation, Software; Muhamad Kamil Yaakob: Visualization, Investigation, Software; Ahmad Azmin Mohamad: Writing- Reviewing and Editing, Soorathep Kheawhom: Writing- Reviewing and Editing

Declaration of competing interest

The authors declare that they have no known competing financial interests or personal relationships that could have appeared to influence the work reported in this paper.

Acknowledgements

The authors wish to thank the Fundamental Research Grant Scheme (FRGS/1/2020/TK0/USM/02/4). for the financial support for this study. B. Deghfel and E. Benrezgua would like to thank the Algerian Ministry of Higher Education and Scientific Research for financial support under the Exceptional National Program (ENP).

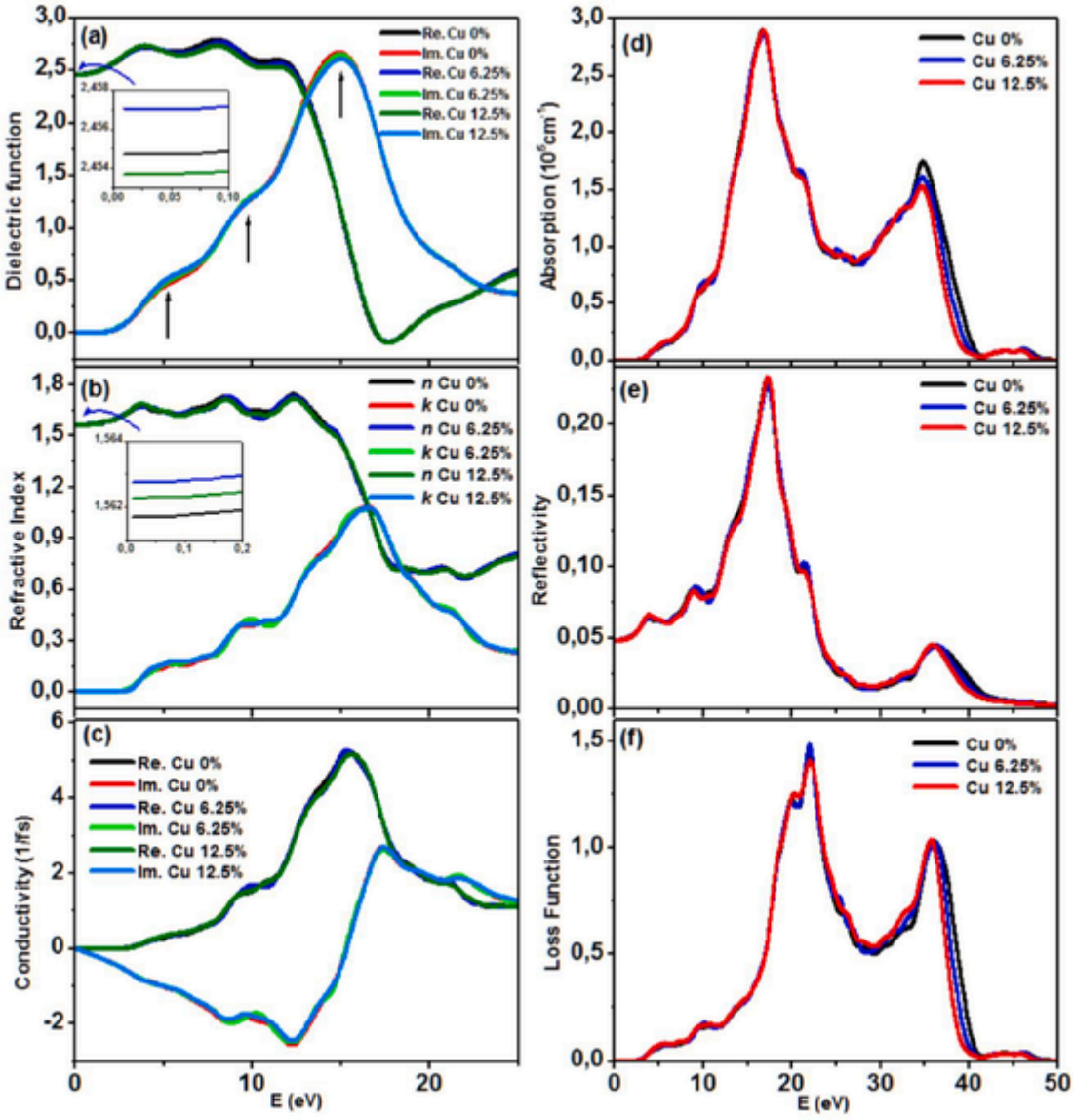

Fig. 8. Complex dielectric function (a), complex refractive index (b), complex conductivity function (c) absorption coefficient (d) optical reflectivity (e) and energy-loss function (f) for pure ZnO and CZO wurtzite structures (x = 6,25%, 12.5%). Inset in (a) shows the evolution of real part of the complex dielectric (ϵ_1) and inset in (b) exhibits the refractive index n for lower photon energy.

References

[1] B.G. Shohany, A.K.J.C.I. Zak, Doped ZnO nanostructures with selected elements-Structural, morphology and optical properties, A review 46 (5) (2020) 5507–5520.

[2] D.R. Miller, S.A. Akbar, P.A. Morris, Nanoscale metal oxide-based heterojunctions for gas sensing: a review, Sensor. Actuator. B Chem. 204 (2014) 250–272.

[3] S. Park, C.-H. Kim, W.-J. Lee, S. Sung, M.-H. Yoon, Sol-gel metal oxide dielectrics for all-solution-processed electronics, Mater. Sci. Eng. R Rep. 114 (2017) 1–22.

[4] A.B. Djurišić, Y.H. Leung, A.M.C. Ng, Strategies for improving the efficiency of semiconductor metal oxide photocatalysis, Materials Horizons 1 (4) (2014) 400–410.

[5] H.A. Al-Khanbashi, W. Shirbeeny, A. Al-Ghamdi, L.M. Bronstein, W.E. Mahmoud, Development of highly conductive and transparent copper doped zinc oxide thin films via 2-methoxyethanol modified sol–gel dip-coating technique, Ceram. Int. 40 (1) (2014) 1927–1932.

[6] W. Vallejo, A. Cantillo, B. Salazar, C. Diaz-Uribe, W. Ramos, E. Romero, M.J.C. Hurtado, Comparative Study of ZnO Thin Films Doped with Transition Metals (Cu and Co) for Methylene Blue Photodegradation under Visible Irradiation 10 (5) (2020) 528.

[7] A. Kronenberger, A. Polity, D.M. Hofmann, B.K. Meyer, A. Schleife, F.J.P.R.B. Bechstedt, Structural, electrical, and optical properties of hydrogen-doped ZnO films 86 (11) (2012) 115334.

[8] R. Amari, A. Mahroug, A. Boukhari, B. Deghfel, N. Selmi, Structural, optical and luminescence properties of ZnO thin films prepared by sol-gel spin-coating method: effect of precursor concentration, Chin. Phys. Lett. 35 (1) (2018) 016801.

[9] A. Mahroug, R. Amari, A. Boukhari, B. Deghfel, L. Guerbous, N. Selmi, Synthesis, structural, morphological, electronic, optical and luminescence properties of pure and manganese-doped zinc oxide nanostructured thin films: effect of doping, J. Nanoelectron. Optoelectron. 13 (5) (2018) 732–742.

[10] D. Shuang, X. Zhu, J. Wang, X. Zhong, G. Huang, C. He, The influence of Mn content on luminescence properties in Mn-doped ZnO films deposited by ultrasonic spray assisted chemical vapor deposition, Appl. Surf. Sci. 257 (14) (2011) 6085–6088.

[11] A. Mhamdi, R. Mimouni, A. Amlouk, M. Amlouk, S. Belgacem, Study of copper doping effects on structural, optical and electrical properties of sprayed ZnO thin films, J. Alloys Compd. 610 (2014) 250–257.

[12] Y. Darma, S. Muhammady, Y.N. Hendri, E. Sustini, R. Widita, K. Takase, Tuning the point-defect evolution, optical transitions, and absorption edge of zinc oxide film by thermal exposure during molecular beam epitaxy growth, Materials Science in Semiconductor Processing 93 (2019) 50–58.

[13] Z.E. Vakulov, E.G. Zamburg, D.A. Khakhulin, O.A. Ageev, Thermal stability of ZnO thin films fabricated by pulsed laser deposition, Materials Science in Semiconductor Processing 66 (2017) 21–25.

[14] W. Thongsuksai, G. Panomsuwan, A.J.M.L. Rodchanarowan, Fast and convenient growth of vertically aligned ZnO nanorods via microwave plasma-assisted thermal evaporation 224 (2018) 50–53.

[15] S. Syed Zahirullah, J. Joseph Prince, P. Fermi Hilbert Inbaraj, Structural and optical properties of Cu-doped ZnO nanorods by silar method, Mater. Technol. 32 (12) (2017) 755–763.

[16] T. Saidani, M. Zaabat, M. Aida, B. Boudine, Effect of copper doping on the photocatalytic activity of ZnO thin films prepared by sol–gel method, Superlattice. Microst. 88 (2015) 315–322.

[17] S. Osali, H. Esfahani, F. Dabir, P. Tajaslan, Structural and electro-optical properties of electrospun Cu-Doped ZnO thin films, Solid State Sci. 98 (2019) 106038.
[18] A. Sreedhar, J.H. Kwon, J. Yi, J.S. Kim, J.S. Gwag, Enhanced photoluminescence properties of Cu-doped ZnO thin films deposited by simultaneous RF and DC magnetron sputtering, Mater. Sci. Semicond. Process. 49 (2016) 8–14.
[19] K. Joshi, M. Rawat, S.K. Gautam, R. Singh, R. Ramola, F. Singh, Band gap widening and narrowing in Cu-doped ZnO thin films, J. Alloys Compd. 680 (2016) 252–258.
[20] S. Roguai, A. Djelloul, A structural and optical properties of Cu-doped ZnO films prepared by spray pyrolysis, Appl. Phys. A 126 (2) (2020) 122.
[21] N.H. Hashim, S. Subramani, M. Devarajan, A.R. Ibrahim, Structural and surface characterization of undoped ZnO and Cu doped ZnO using sol–gel spin coating method, J. Mater. Sci. Mater. Electron. 27 (4) (2016) 3520–3530.
[22] A.R. Nimbalkar, M.G. Patil, Synthesis of highly selective and sensitive Cu-doped ZnO thin film sensor for detection of H2S gas, Mater. Sci. Semicond. Process. 71 (2017) 332–341.
[23] P. Shewale, Y. Yu, UV photodetection properties of pulsed laser deposited Cu-doped ZnO thin film, Ceram. Int. 43 (5) (2017) 4175–4182.
[24] G.-J. Chen, S.-R. Jian, J.-Y. Juang, Surface analysis and optical properties of Cu-doped ZnO thin films deposited by radio frequency magnetron sputtering, Coatings 8 (8) (2018) 266.
[25] J.-H. Lee, K. Oh, K. Jung, K. Wilson, M.-J. Lee, Tuning the morphology and properties of nanostructured Cu-ZnO thin films using a two-step sputtering technique, Metals 10 (4) (2020) 437.
[26] N. Narayanan, N. Deepak, Enhancement of visible luminescence and photocatalytic activity of ZnO thin films via Cu doping, Optik 158 (2018) 1313–1326.
[27] V.I. Anisimov, F. Aryasetiawan, A. Lichtenstein, First-principles calculations of the electronic structure and spectra of strongly correlated systems: the LDA + U method, J. Phys. Condens. Matter 9 (4) (1997) 767.
[28] M. Yaakob, N. Hussin, M. Taib, T. Kudin, O. Hassan, A. Ali, M. Yahya, First principles LDA + U calculations for ZnO materials, Integrated Ferroelectrics Int. J. 155 (1) (2014) 15–22.
[29] J.-Q. Wen, J.-M. Zhang, Z.-G. Qiu, X. Yang, Z.-Q. Li, The investigation of Ce doped ZnO crystal: the electronic, optical and magnetic properties, Phys. B Condens. Matter 534 (2018) 44–50.
[30] Q. Hou, D. Xi, W. Li, X. Jia, Z. Xu, First-principles research on the optical and electrical properties and mechanisms of In-doped ZnO, Phys. B Condens. Matter 537 (2018) 258–266.
[31] Z. Ma, F. Ren, X. Ming, Y. Long, A.A. Volinsky, Cu-doped ZnO electronic structure and optical properties studied by first-principles calculations and experiments, Materials 12 (1) (2019) 196.
[32] F. Li, C. Zhang, M. Zhao, Magnetic and optical properties of Cu-doped ZnO nanosheet: first-principles calculations, Phys. E Low-dimens. Syst. Nanostruct. 53 (2013) 101–105.
[33] L. Chen, S. Li, Y. Cui, Z. Xiong, H. Luo, Y. Gao, Manipulating the electronic and magnetic properties of ZnO monolayer by noble metal adsorption: a first-principles calculations, Appl. Surf. Sci. 479 (2019) 440–448.
[34] A.K. Nayek, H. Luitel, B. Haldar, D. Sanyal, M. Chakrabarti, Ferromagnetic property of copper doped ZnO: a first-principles study, Computational Condensed Matter 23 (2020) e00455.
[35] C. Xia, F. Wang, C. Hu, Theoretical and experimental studies on electronic structure and optical properties of Cu-doped ZnO, J. Alloys Compd. 589 (2014) 604–608.
[36] D. Fang, A. De Sarkar, R. Zhang, First-principles study on the origin of ferromagnetism in n-type Cu-doped ZnO, Solid State Commun. 152 (12) (2012) 1057–1060.
[37] C. Feng, Z. Chen, W. Li, F. Zhang, X. Li, L. Xu, M. Sun, First-principle calculation of the electronic structures and optical properties of the metallic and nonmetallic elements-doped ZnO on the basis of photocatalysis, Phys. B Condens. Matter 555 (2019) 53–60.
[38] S. Sriram, K. Lalithambika, A. Thayumanavan, Experimental and theoretical investigations of photocatalytic activity of Cu doped ZnO nanoparticles, Optik 139 (2017) 299–308.
[39] M. Lahmer, The effect of hydrogen adsorption on the properties of undoped and Cu-doped ZnO ($10\bar{1}$ 0) surfaces: a first-principles study, J. Phys. Chem. Solid. 89 (2016) 89–96.
[40] Q. Wang, J. Wang, X. Zhong, Q. Tan, Y. Zhou, The magnetic phase transition in Cu-doped ZnO: from bulk to nanocluster, Solid State Commun. 152 (1) (2012) 50–52.
[41] Z. Long, L. Peng-Fei, Y. Zhong-Yuan, L. Yu-Min, W. Dong-Lin, Y. Han, First-principles study of electronic and optical properties in wurtzite Zn1–xCuxO, Chin. Phys. B 19 (5) (2010) 056104.
[42] B.-S. Kang, K.-S. Kim, S.-C. Yu, H. Chae, First-principles study for ferromagnetism of Cu-doped ZnO with carrier doping, J. Solid State Chem. 198 (2013) 120–124.
[43] V. Mendoza-Estrada, A. González-García, D. Barragán-Yani, W. López-Pérez, J. Rivera-Julio, R. González-Hernández, Ferromagnetic orderings in CoxCuyZn1−(x + y) O by GGA and GGA + U formalisms within density functional theory, Comput. Mater. Sci. 126 (2017) 344–350.
[44] S.J. Clark, M.D. Segall, C.J. Pickard, P.J. Hasnip, M.I. Probert, K. Refson, M.C. Payne, First principles methods using CASTEP, Z. für Kristallogr. - Cryst. Mater. 220 (5–6) (2005) 567–570.
[45] J.P. Perdew, K. Burke, M. Ernzerhof, Generalized gradient approximation made simple, Phys. Rev. Lett. 77 (18) (1996) 3865.
[46] R. Amari, B. Deghfel, A. Mahroug, A.A. Mohamad, A. Boukhari, N. Selmi, Effects of Mn doping on the structural, morphological, electronic and optical properties of ZnO thin films by sol-gel spin coating method: an experimental and DFT + U study, Phys. B Condens. Matter 577 (2020) 411766.
[47] D. Vanderbilt, Soft self-consistent pseudopotentials in a generalized eigenvalue formalism, Phys. Rev. B 41 (11) (1990) 7892.
[48] V. Mendoza-Estrada, W. López-Pérez, R. González-Hernández, A. González-García, Electronic Structure and Magnetic Order in CuxZn (1− x) O: A study GGA GGA + U. Phys. B Condens. Matter 557 2019 74 81
[49] D.V. Vu, D.H. Le, T.T. Nguyen, T. Van Duong, Q.D. Ngo, T.Q. Trinh, Study on material properties of Sn-and Cu-doped ZnO thin films as n-and p-type thermoelectric materials based on wet solution synthesis, Journal of Materials Science: Materials in Electronics 30 (7) (2019) 6544–6551.
[50] I. Horcas, R. Fernández, J. Gomez-Rodriguez, J. Colchero, J. Gómez-Herrero, A. Baro, WSXM: a software for scanning probe microscopy and a tool for nanotechnology, Rev. Sci. Instrum. 78 (1) (2007) 013705.
[51] M. Salem, I. Massoudi, S. Akir, Y. Litaiem, M. Gaidi, K. Khirouni, Photoelectrochemical and opto-electronic properties tuning of ZnO films: effect of Cu doping content, J. Alloys Compd. 722 (2017) 313–320.
[52] S.C. Endres, L.C. Ciacchi, L. Mädler, A Review of Contact Force Models between Nanoparticles in Agglomerates, Aggregates, and Films, 153, Journal of Aerosol Science, 2020 105719.
[53] S. Yang, Y. Zhang, D.J.T.S.F. Mo, Spectroscopic ellipsometry studies of sol-gel-derived Cu-doped ZnO thin films 571 (2014) 605–608.
[54] P. Jongnavakit, P. Amornpitoksuk, S. Suwanboon, N.J.A.S.S. Ndiege, Preparation and photocatalytic activity of Cu-doped ZnO thin films prepared by the, Sol–gel method 258 (20) (2012) 8192–8198.
[55] A. El Sayed, G. Said, S. Taha, A. Ibrahim, F.J.S. Yakuphanoglu, Microstructures, Influence of copper incorporation on the structural and optical properties of ZnO nanostructured thin films 62 (2013) 47–58.
[56] L. Xu, F. Xian, G. Zheng, M.J.M.R.B. Lai, Realization of strong violet and blue emissions from ZnO thin films by incorporation of Cu ions 99 (2018) 144–151.
[57] M. Mazhdi, J. Saydi, M. Karimi, J. Seidi, F.J.O. Mazhdi, A study on optical, photoluminescence and thermoluminescence properties of ZnO and Mn doped-ZnO nanocrystalline particles 124 (20) (2013) 4128–4133.
[58] Y. Kim, J.-Y. Leem, Effects of precursor concentration on structural and optical properties of ZnO thin films grown on muscovite mica substrates by sol–gel spin-coating, J. Nanosci. Nanotechnol. 16 (5) (2016) 5186–5189.
[59] A. Saboor, S.M. Shah, H. Hussain, Band gap tuning and applications of ZnO nanorods in hybrid solar cell: Ag-doped verses Nd-doped ZnO nanorods, Materials Science in Semiconductor Processing 93 (2019) 215–225.
[60] Y. Liu, H. Liu, Y. Yu, Q. Wang, Y. Li, Z. Wang, Structural and optical properties of ZnO thin films with heavy Cu-doping prepared by magnetron co-sputtering, Mater. Lett. 143 (2015) 319–321.
[61] V. Ganesh, G. Salem, I. Yahia, F. Yakuphanoglu, Synthesis, optical and photoluminescence properties of Cu-doped ZnO nano-fibers thin films: nonlinear optics, J. Electron. Mater. 47 (3) (2018) 1798–1805.
[62] M. Sajjad, I. Ullah, M. Khan, J. Khan, M.Y. Khan, M.T. Qureshi, Structural and optical properties of pure and copper doped zinc oxide nanoparticles, Results in Physics 9 (2018) 1301–1309.
[63] M. DrDomenico Jr., S.H. Wemple, Oxygen-octahedra ferroelectrics. I. Theory of electro-optical and nonlinear optical effects, Journal of Applied Physics 40 (2) (1969) 720–734.
[64] Y.J.J. o. a. Caglar, Compounds, Sol–gel derived nanostructure undoped and cobalt doped ZnO: Structural, optical and electrical studies 560 (2013) 181–188.
[65] E.Ş. Tüzemen, S. Eker, H. Kavak, R.J.A.S.S. Esen, Dependence of film thickness on the structural and optical properties of ZnO thin films 255 (12) (2009) 6195–6200.
[66] A. Ciechan, P.J.O.M. Bogusławski, Transition metal ions in ZnO: Effects of intrashell coulomb repulsion on electronic properties 79 (2018) 264–268.